

Kerr-Induced Synchronization of a Cavity Soliton to an Optical Reference

Grégory Moille,^{1,2,*} Jordan Stone,^{1,2} Michal Chojnacky,^{1,3} Rahul Shrestha,¹ Usman A. Javid,^{1,2} Curtis Menyuk,⁴ and Kartik Srinivasan^{1,2,†}

¹*Joint Quantum Institute, NIST/University of Maryland, College Park, USA*

²*Microsystems and Nanotechnology Division, National Institute of Standards and Technology, Gaithersburg, USA*

³*Sensor Science Division, National Institute of Standards and Technology, Gaithersburg, USA*

⁴*University of Maryland at Baltimore County, Baltimore, MD, USA*

(Dated: September 3, 2023)

The phase-coherent frequency division of a stabilized optical reference laser to the microwave domain is made possible by optical frequency combs (OFCs) [1, 2]. OFC-based clockworks [3–6] lock one comb tooth to this reference laser, which probes a stable atomic transition, usually through an active servo that increases the complexity of OFC photonic and electronic integration for fieldable clock applications. Here, we demonstrate that the Kerr nonlinearity enables passive, electronics-free synchronization of a microresonator-based dissipative Kerr soliton (DKS) OFC [7] to an externally-injected reference laser. We present a theoretical model that explains this Kerr-induced synchronization (KIS) and closely matches experiments based on a chip-integrated, silicon nitride microring resonator. Once synchronized, the reference laser captures an OFC tooth, so that its frequency tuning provides direct external control of the OFC repetition rate. We also show that the repetition rate stability is linked to that of the reference laser through the expected frequency division factor. Finally, KIS of an octave-spanning DKS exhibits enhancement of the opposite dispersive wave, consistent with the theoretical model, and enables improved self-referencing and access to the comb carrier-envelope offset frequency. The KIS-mediated enhancements we demonstrate can be directly implemented in integrated optical clocks and chip-scale low noise microwave generation.

Optical frequency combs (OFCs) provide a phase-coherent link between the optical and microwave domains and are the foundation for metrology applications such as optical synthesizers [8, 9] and distance ranging [10, 11]. OFCs play a critical role in time-keeping [1], enabling a transition from microwave frequency Cs atomic clocks [12] to optical atomic clocks [3]. These clocks rely on a stable laser locked to an environmentally-insensitive optical transition [4–6] and use OFCs as optical-to-microwave frequency dividers [2], with the clock output being the OFC repetition rate [13, 14]. Integrated photonics now offers on-chip optical clockworks [15, 16], primarily via OFCs based on dissipative Kerr solitons (DKS) in microring resonators [7], in particular harnessing octave-spanning operation and so-called dispersive wave generation [17–20]. Whether the OFCs are on a chip or not, the clockwork for optical frequency division entails the active locking of a single OFC comb tooth to the reference laser. Though there has been much progress in developing electronics associated with OFC applications [21, 22], the power budget and limited bandwidth associated with such active stabilization represents a barrier to full integration of an optical clock, even if the power required to optically drive the integrated OFC can be extremely low [23].

In this work, we show that by injecting the reference laser into a DKS microresonator – hence turning it into another pump for the DKS system – an all-optical, passive Kerr-induced synchronization (KIS) of the OFC to the reference laser is achieved. Nonlinear Kerr phase locking

of the DKS to the reference pump laser is demonstrated by using a microresonator with the appropriate dispersion for dispersive wave generation at the reference pump frequency. Our experiments are supported by close agreement with Lugiato-Lefever equation simulations, and we further develop an expanded Adler equation that describes the requirements for synchronization and its behavior. When synchronized, the reference pump is effectively part of the DKS, and we accordingly show that the DKS repetition rate may be adjusted on demand by detuning the reference pump, following a frequency division ratio set by the number of comb teeth between the two pumps. Lastly, we apply KIS to an octave-spanning microcomb and improve its carrier-envelope offset frequency accessibility through the f - $2f$ technique. In particular, not only is doubling of the low frequency dispersive wave comb tooth made orders of magnitude more efficient due to use of the reference laser, the opposite (high frequency) dispersive wave is also increased in power, due to a novel soliton self-balancing effect.

The analogy between optical and mechanical clocks [1] in which the OFC is likened to gears is often drawn [Fig. 1], and helps explain the context of our work. The development of the mechanical pendulum clock, notably Shortt’s model [24], was a hallmark of precision in its time. It avoided mechanical damping, a major stability issue, by locking a follower pendulum to a vacuum-sealed reference [Fig. 1a]. Modern OFC clockworks mirror this architecture. While synchronization can be an alternative to active locking, as shown by Huygens with coupled pendulums [Fig. 1b], this approach has stability issues in mechanical systems due to increased damping. Yet, optical clocks differ notably in damping mechanisms. They can utilize

* gregory.moille@nist.gov

† kartik.srinivasan@nist.gov

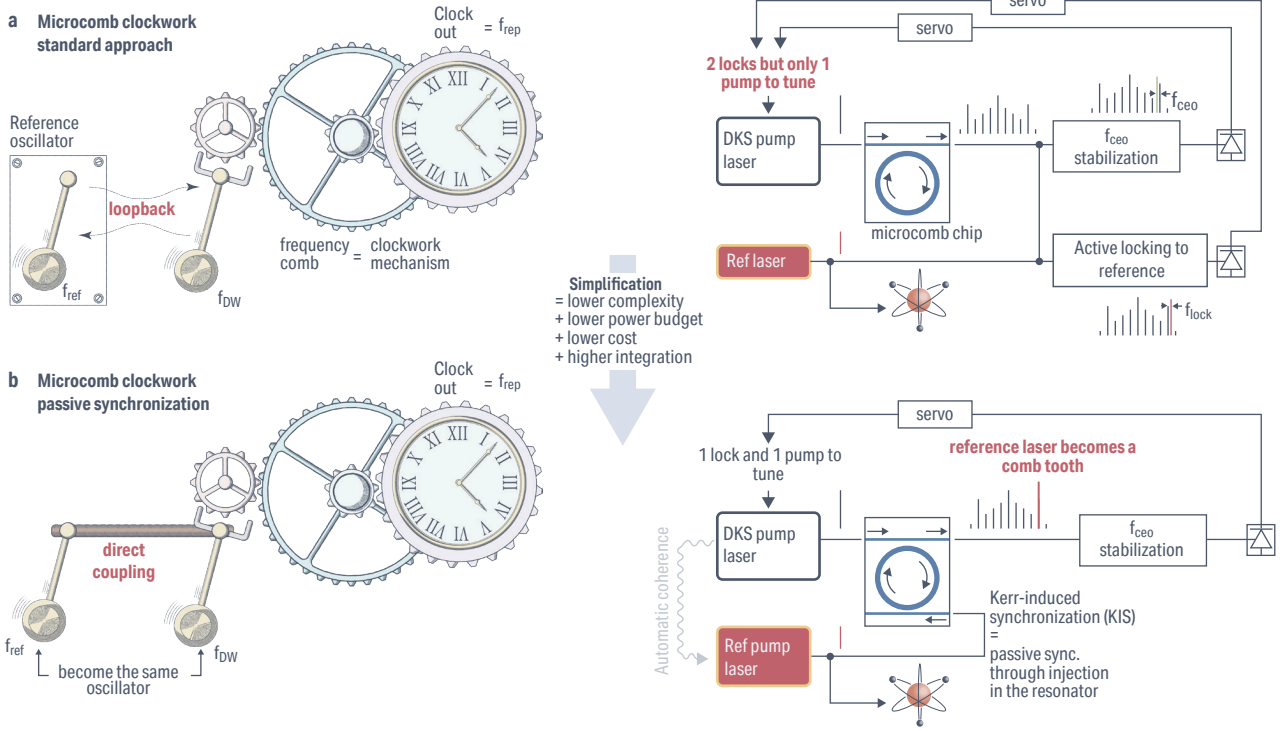


Fig. 1

mostly lossless optical nonlinearities for long-term synchronization, seen in phenomena like counter-propagating DKSs in microresonators [25]. An OFC design using Kerr-induced nonlinear coupling for passive synchronization could greatly simplify optical clock systems.

Theoretical framework — Before delving into the experimental findings, it is necessary to recall the DKS behavior under various driving conditions. The DKS’s two fundamental characteristics are its group and phase velocity. The repetition rate, ω_{rep} , arises from the group velocity, and specifies the temporal separation between two extracted pulses in the bus waveguide. The DKS phase velocity is connected to the carrier-envelope offset (CEO), which is a phase slip $\varphi(t)$ of the rapid oscillation below the envelope for each extracted pulse, and results in the CEO frequency $\omega_{\text{ceo}} = \partial\varphi/\partial t$ [Fig. 2a]. Introducing the reference pump laser to the cavity forms a secondary pulse, resulting in a multi-color soliton (MDKS) with uniform group velocity through cross-phase modulation binding [26, 27]. As a result of the single group velocity MDKS, any comb formed around the reference pump will have the same ω_{rep} as the DKS OFC. To accomplish effective power transfer inside the cavity, the reference must be on resonance when it is injected into the microring. However, the two components of the MDKS will in general have different phase velocities that are determined by cavity dispersion, leading to a non-zero CEO frequency shift between these two comb components $\Omega = \omega_{\text{ref}} - \omega_{\mu_s} = \partial\Phi/\partial t$ [Fig. 2b - top], where $\Phi = \varphi_{\text{ref}} - \varphi_{\text{dks}}$, and ω_{μ_s} is the frequency at mode μ_s (the comb tooth closest to the reference pump frequency). This

can be harnessed for spectral extension [28] or creation of advanced combs [27]. These demonstrations are intriguing, but by definition, systems exhibiting $\Omega = \partial\Phi/\partial t \neq 0$ are not synchronized. Until now, multi-driving of a DKS has only been observed when the primary and secondary combs are unsynchronized [27–30] and when soliton crystals are generated [31, 32]. Here, we investigate the specific conditions to achieve phase locking and demonstrate its appearance.

Synchronization between oscillators can be understood using an Adler equation, for which an extended version can be obtained for a DKS under multiple driving fields (see Supplementary S1), such that:

$$-\frac{1}{\kappa} \frac{\partial^2 \Phi}{\partial t^2} - \frac{\partial \Phi}{\partial t} = D_{\text{int}}(\mu_s) + \Delta - \mathcal{T} \sin(\Phi) \quad (1)$$

which is the equation of motion of a damped pendulum under constant torque driving [33], here with μ the azimuthal order referenced to the main pump, $\Delta = \delta\omega_{\text{ref}} + \mu_s D_1(\mu_0)(1 + K_{\text{NL}} - K_0)$ the effective reference pump detuning with $\delta\omega_{\text{ref}}$ being the detuning of the reference pump, $K_0 = \frac{2|A(\mu_0)|}{E_{\text{DKS}}} \sqrt{\frac{P_{\text{main}} \kappa_{\text{ext}}}{\kappa^2}}$ the normalized XPM phase shift induced by the mode μ_j , P_{ref} and E_{dks} are the power and energy of the reference and the DKS respectively, $D_1(\mu_j)$ is the linear free spectral range at the azimuthal component μ_j , K_{NL} accounts for the cross-phase modulation induced by the MDKS (see Supplementary S1), κ and κ_{ext} are the total and coupling losses, respectively, μ_s is the azimuthal mode at which the reference is synchronized, and $\mathcal{T} = D_1(\mu_s) \mu_s \frac{2|A(\mu_s)|}{E_{\text{DKS}}} \sqrt{\frac{P_{\text{ref}} \kappa_{\text{ext}}}{\kappa^2}}$ is

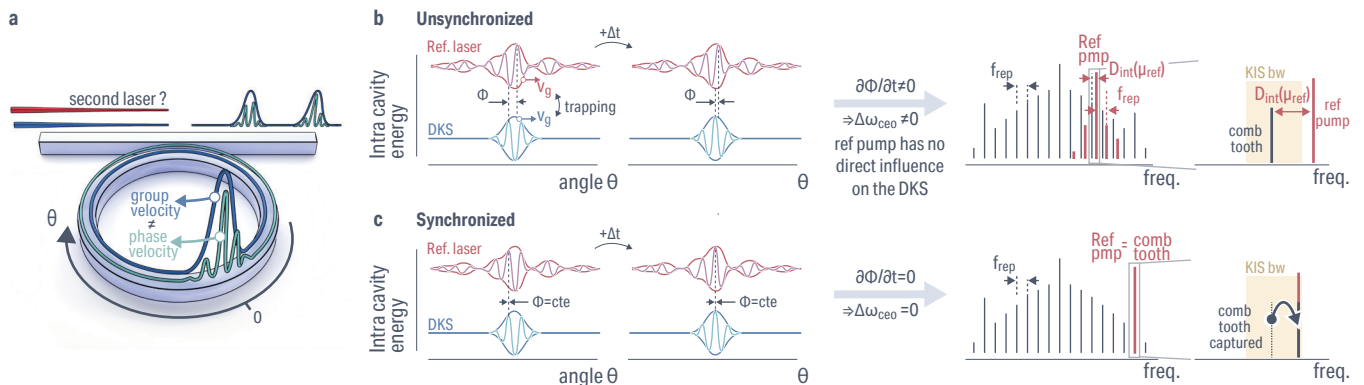


Fig. 2

the effective natural torque of the system. Eq. (1) is similar to the equation for counter-propagating DKSs [25], though our synchronization arises from an external force. Synchronization happens when the left side of Eq. (1) is null, requiring compensation of $D_{\text{int}}(\mu_s)$ by either the nonlinear shift or reference pump detuning. Achieving this via a CEO offset from $D_{\text{int}}(\mu_s)$ compensated by XPM is theoretically feasible, but its requirements on high power and phase shift balance make experimental demonstration challenging. However, minimizing $D_{\text{int}}(\mu_s)$ reduces the required reference pump power for synchronization.

Octave-spanning microcombs rely on the generation of dispersive waves (DWs) to extend the comb spectrum, thanks to high-order dispersion terms becoming commensurate with the the group velocity dispersion. In this scenario, the integrated dispersion $D_{\text{int}}(\mu) = \sum_{k>1} \frac{D_k}{k!} \mu^k = \omega_{\text{res}}(\mu) - (\omega_{\text{pmp}} + D_1\mu)$ presents multiple zero crossings that provide phase matching for the DW creation, notably in the normal dispersion regime of the resonator. Thus, D_{int} is minimized at the DW mode, allowing for synchronization to occur, while also allowing the reference pump to be in the normal dispersion regime where soft-excited bright DKS states cannot be generated. This prevents both multi-DKS states and modulation instability states directly driven by the reference pump. The synchronization effect could also be considered under the prism of inhomogeneity trapping of the cavity soliton, where the reference pump creates a background modulation whose inhomogeneity captures the DKS envelope [34]. Such an effect is shown in systems with cavity drift control [35] and a synthetic frequency lattice [36].

Optical characterization of the synchronization

— Our system under study is a resonator with a $23 \mu\text{m}$ outer radius that is made of $H = 670 \text{ nm}$ thick Si_3N_4 with a ring width of $RW = 830 \text{ nm}$ embedded in SiO_2 . It has an anomalous dispersion when pumped at 286 THz (1048 nm), and this design yields an octave-spanning bandwidth while reaching the rubidium two-photon transition at $\approx 386 \text{ THz}$ [5, 20]. We characterize the dispersion of the fundamental transverse electric mode of the cavity using multiple continuously tunable lasers (CTLs) and calibrate each resonance using a wavemeter. The measured $D_{\text{int}}(\mu)$ matches expectation from simulation, with

a DW at $\omega_{\text{DW}}/2\pi \approx 194 \text{ THz}$ (1544 nm , $\mu_{\text{DW}} = -92$) [Fig. 3a]. The high-frequency DW at $\approx 384 \text{ THz}$ is not out-coupled as the pulley coupler length $L_c = 28 \mu\text{m}$ is optimized for critical coupling of both the main pump and low-frequency DW. We actively cool the resonator using a counter-propagating cross-polarized 308 THz (974 nm) laser, allowing for adiabatic detuning of the pump to reach the single DKS state [27, 37, 38], which we obtain with an on-chip pump power of about 150 mW . To study system synchronization, we use a CTL parked at different modes μ and fine-tune its detuning to observe the impact of $\delta\omega_{\text{ref}}$ [Fig. 3b]. A distinct optical behavior emerges with varying $\delta\omega_{\text{ref}}$. At resonance, comb lines around μ_{DW} are pronounced, exceeding the 4 GHz analyzer resolution and producing a 2D comb [27], indicating an unsynchronized state. Adjusting $\delta\omega_{\text{ref}}$ decreases the power of these comb lines, hinting at a synchronized state when their value increase again due to the merging of the multi-color DKS [Fig. 3b - sync case]. We proceed to record Ω – obtained by measuring the comb with a fast photodiode and processed with an electrical spectral analyzer – with the reference pump detuning $\delta\omega_{\text{ref}}$ [Fig. 3c], to demonstrate the synchronization dynamics of the system. The reference pump is centered at $\mu = -92$ and has $\approx 2 \text{ mW}$ of on-chip power. Out of synchronization, a beat note $\Omega \neq 0$ is recorded between the reference laser and the nearest comb tooth, as they are distinct, with Ω varying linearly with $\delta\omega_{\text{ref}}$. The trend becomes hyperbolic once the laser is adjusted sufficiently close to the KIS window, similar to Appleton’s first observation of synchronization in his triode oscillator [39]. Then Ω vanishes, indicating that KIS has occurred, over a range of $\delta\omega_{\text{ref}} \approx 1.75 \text{ GHz}$. We also find that the Lugiato-Lefever equation (LLE) model under multi-driving fields introduced in ref. [40] captures this KIS behavior accurately. In that work, though the second pump was situated in anomalous dispersion, which greatly limits experimental demonstration in contrast to pumping at the DW mode, the authors theoretically showed that an external laser different from the main pump may become a comb tooth, allowing for control of the repetition rate. Using the *pyLLE* freeware [41], we accurately reproduce the experimentally-observed behavior of the CEO offset Ω (see Methods). Following Eq. (1), the KIS bandwidth

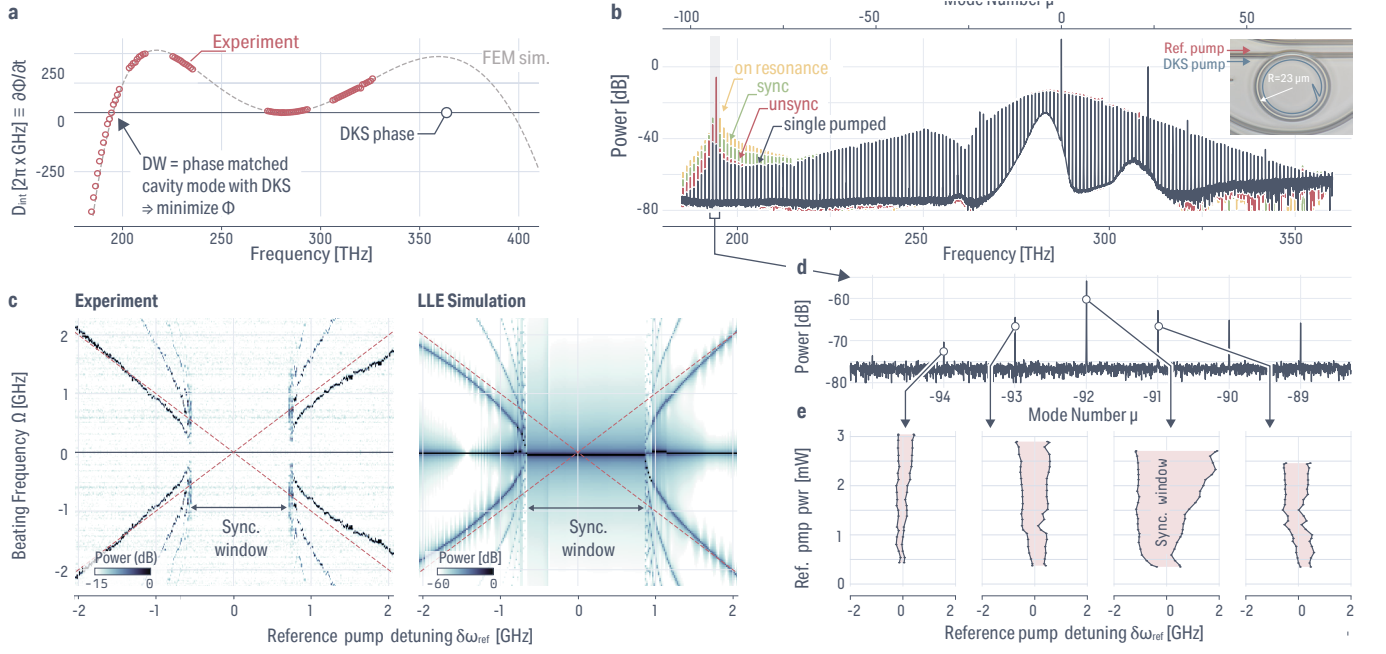


Fig. 3

$\Delta\omega_{\text{lock}} \propto \sqrt{|A_{\mu,s}|^2 P_{\text{ref}}}$ is proportional to the μ^{th} DKS component power that locks with the reference; hence for a given μ and reference power, the KIS window is maximal exactly at the DW [Fig. 3d]. We reproduce this behavior experimentally by probing several modes around the DW at $\mu = -92$ for different reference pump power as low as ≈ 300 μW on chip [Fig. 3e]. We note that we have normalized the detuning relative to the center of the KIS window, as under DKS operation, obtaining the exact resonance position is experimentally challenging. All the measurements have been performed with a reference pump detuning from red (lower frequency) to blue (higher frequency). The same synchronization effect happens with a reversed detuning direction, where a hysteresis behavior in the Arnold tongue frequency is observed (see Supplementary Material S3).

External control of the soliton repetition rate — Since $\partial\Phi/\partial t = 0$ in the KIS state, any variations in the reference frequency are divided onto the repetition rate such that $\partial(\delta\omega_{\text{ref}})/\partial\omega = \mu_s \partial\omega_{\text{rep}}/\partial\omega$, assuming that the main pump is fixed (see Supplementary S1). As a result, the azimuthal mode difference μ_s between the primary pump and the reference pump defines the frequency division factor in this dual-pinned comb. Therefore, by adjusting the detuning of the reference pump while synchronizing with the DKS, one could adjust its repetition rate without interfering with the main pump parameters [Fig. 4a]. The Adler equation predicts this frequency division, yet we also verify it using the LLE model. We tune the reference pump frequency for the azimuthal mode $\mu_s = -89$ and extract the repetition rate (see Methods). Upon reaching the KIS state, the closest comb tooth aligns with the reference pump frequency, changing abruptly ω_{rep} [Fig. 4b]. The DKS repetition rate then linearly varies with the

reference detuning within the synchronization range. This slope matches the expected frequency division based on the azimuthal mode number difference, which we validate for several other μ_s values.

To experimentally demonstrate such an effect, we must accurately measure the repetition rate of the OFC, which is generally not directly achievable with a terahertz repetition rate octave-spanning microcomb. We use an electro-optic comb apparatus (see Methods) to effectively translate two adjacent comb teeth and produce a detectable frequency beat [Fig. 4c]. Using this method, we demonstrate that the slope of the linear trend of the repetition rate shift with the reference frequency matches the mode difference between the DKS pump and the reference pump, and is in accordance with the frequency division principle for several azimuthal modes [Fig. 4d]. The KIS windows are different for each azimuthal mode, as the comb tooth power in the DKS is not constant with the probed μ .

It is worth discussing the KIS regime in the context of recent research on self-injection locking for seamless DKS generation [42, 43]. In such injection locking techniques, the DKS resonator's backscattered signal is fed back into the (isolator-free) laser system, tuning and locking the laser frequency according to the intracavity's most favorable regime. In KIS, the reverse effect occurs. Rather than modifying the laser frequency for locking, our reference pump (with isolators) maintains a constant frequency and instead forces the DKS to adjust its azimuthal component frequencies to meet the locking prerequisites. The experimental tuning of the DKS repetition rate underscores this phenomenon.

Stability transfer for clockwork operation — We experimentally demonstrate the viability of the Kerr-induced synchronization approach for clockwork applica-

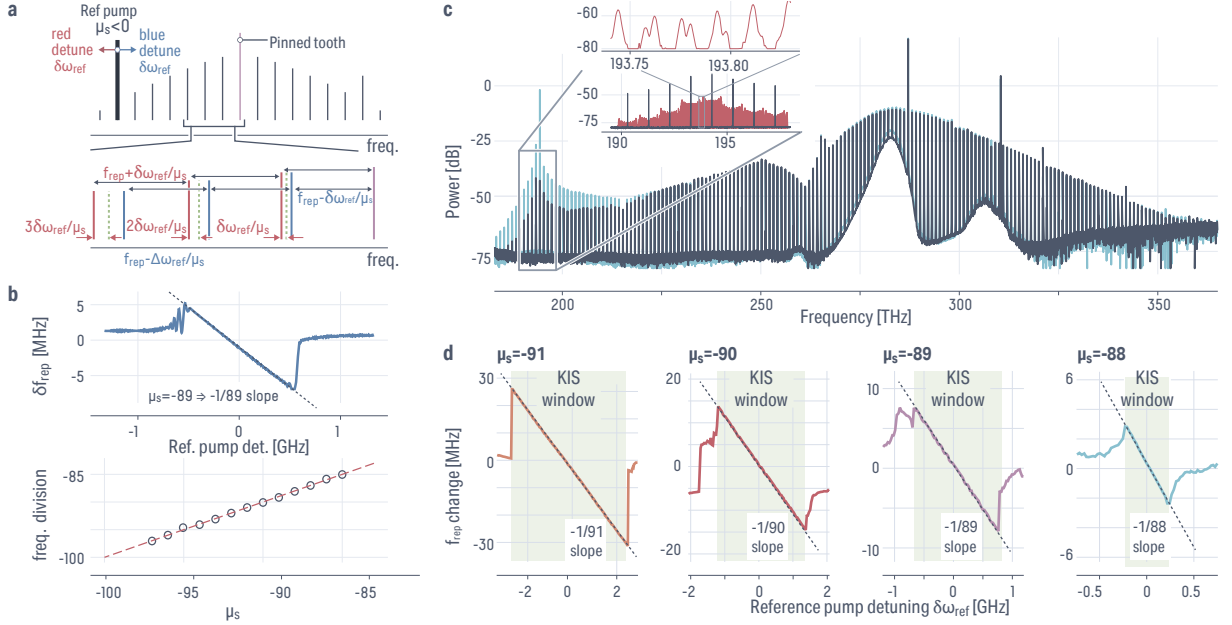


Fig. 4

tions. Although we have demonstrated frequency division in the previous section [Fig. 4], we now study short and long-term stability of the DKS repetition rate relative to the reference. As the current OFC under study prevents CEO stabilization via $f - 2f$ (the short DW is not extracted), we use a Toptica Photonics CEO-free fiber comb with a 80 MHz repetition rate that is referenced to a 10 MHz Rubidium standard [44, 45]. Once both the main and reference pump are locked to this comb, their frequency separation becomes coherently linked to the Rb reference. Hence, when the DKS is in the KIS regime, a frequency division factor links the DKS repetition rate to the pump separation and, in turn, the Rb reference. However, rather than the full frequency division if the DKS CEO is locked, a frequency division factor μ_s between the two pinned comb lines is achieved.

First, we demonstrate that the repetition rate is indeed much more stable in the synchronized case [Fig. 5a]. Without KIS, the repetition rate is relatively unstable, with a full-width at half-maximum (FWHM) exceeding 160 kHz at a recording bandwidth of 1 Hz. In the KIS regime with free-running pumps, the FWHM is around 11 kHz FWHM, consistent with the slow (≈ 10 s) scanning time of the spectrum analyzer, the pump laser linewidths in this time frame (i.e. ≈ 500 MHz each), and the frequency division factor $\mu_s = -92$. However, once both pumps are locked to the fiber comb using a phase frequency detector with fast analog control [46], hence achieving coherence with the Rb reference, the repetition rate becomes Lorentzian and narrows to about 3 Hz. The temporal frequency counting trace of the repetition rate measurement with a gate time of 10 ms is presented in Fig. 5b, highlighting a 12 Hz standard deviation from the 997,387,327,768 Hz microcomb repetition rate.

We measure the phase noise of the repetition rate and

the reference pump to further demonstrate the fidelity of synchronization for frequency division. In this experiment, we lock the main pump to the fiber comb. To highlight that the phase noise of the reference is divided onto the DKS repetition rate we leave the reference pump free running (Fig. 5c), while the main pump noise contribution is negligible. After accounting for frequency division factor, the reference pump phase noise overlaps with the measured repetition rate phase noise as expected.

To further demonstrate the potential of the passive synchronization approach for clockwork application, we measure the long-term stability of the system by measuring the repetition rate Allan deviation [Fig. 5d]. The $1/\tau$ trend at long averaging time suggests contributions only from white phase noise, demonstrating coherence with the 80 MHz fiber comb.

We show a residual stability of 1 part in 1.25×10^{12} at 1 second, similar to the fiber comb stability at 1 second and demonstrating the stability division, and 1 part in 10^{14} at 50 minutes. The plateau between 1 s and 10 s is likely caused by environmental factors, such as the long electronic path in the locking loop, which leads to impedance mismatch and spurious reflections. This is consistent with previous observations using active locking [16], and hence is not inherent to the KIS regime. We note that the stability metric may be influenced by several factors, including our complex frequency division scheme [Fig. 5d], and can be enhanced by simplifying the feedback mechanism and using self-referencing in the future, removing the need for the fiber comb.

Carrier envelope offset detection enabled by KIS

— Finally, we discuss the advantages of the Kerr-induced synchronization regime for self-referencing the microcomb. In an optical clockwork, it is necessary to anchor two comb teeth, with one pinned to the optical reference. Locking the

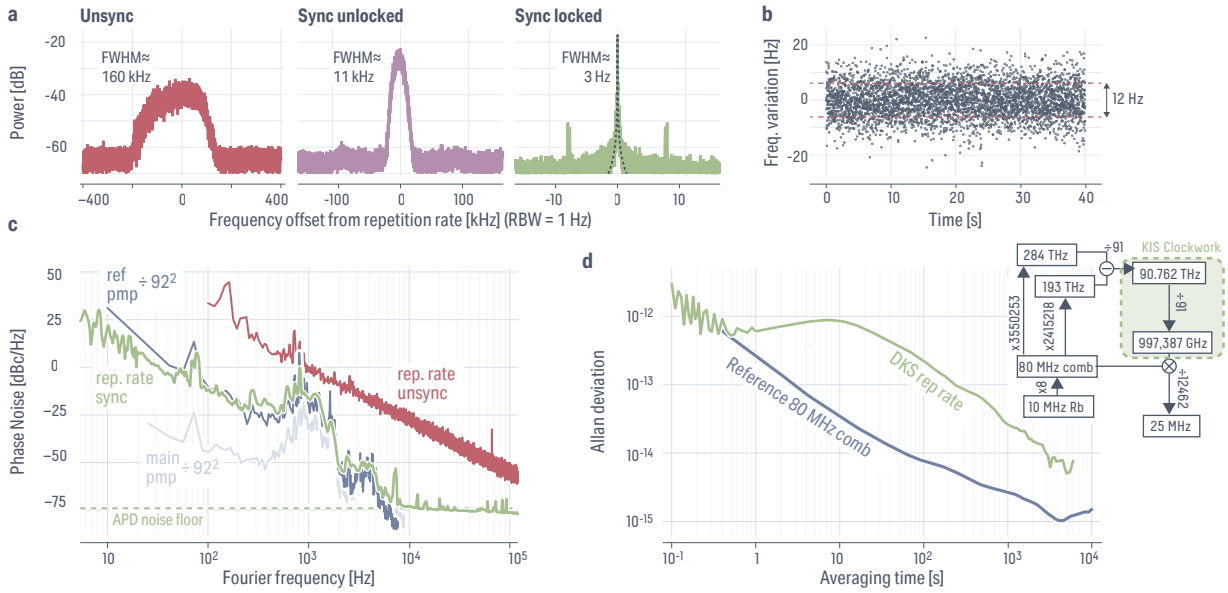


Fig. 5

CEO is equivalent to locking the first comb line, providing the largest frequency division ratio possible. The CEO frequency is obtained from a nonlinear interferometer that beats two harmonic comb teeth, where one is doubled: $2\omega_N - \omega_{2N} = 2(N\omega_{\text{rep}} + \omega_{\text{ceo}}) - 2N\omega_{\text{rep}} - \omega_{\text{ceo}} = \omega_{\text{ceo}}$. In integrated frequency combs, despite the presence of DWs, the power at these frequencies of interest is usually low. Consequently, an auxiliary laser needs to be locked for efficient doubling and detection [9, 15], increasing the amount of required locking electronics. However, in the KIS regime, the reference laser that captures a comb tooth can be directly used for CEO detection. This provides sufficient power, with amplification capacity for generating a large doubled power. Furthermore, the locking of the reference laser to a Rb frequency standard often involves a doubled narrow-linewidth telecom laser to address, for example, the Rb two-photon transition [5], which means that both the second harmonic generation (SHG) module and a telecom-band reference laser are already present in the clock architecture.

The KIS regime also offers a unique method to increase the power of the opposite DW from where the synchronization occurs. Any change in reference pump in Eq. (1) needs to be compensated by other terms to maintain a null left-hand side. K_{NL} , which includes the power of every soliton azimuthal component, is the only free parameter. Given that the soliton spectral envelope is fixed by the dispersion, the only comb tooth which can vary is at the DW. Hence, to maintain balance, the soliton boosts its emission into the opposite DW, increasing short-wavelength DW power. This can also be seen as the soliton maintaining its pinned repetition rate from the pumps and the need to maintain a constant center-of-mass, resulting in self-balancing (see extended data ??). Thus, CEO detection is improved in two ways in the KIS regime.

We proceeded to measure CEO experimentally using

a similar microring resonator as in the previous section, with a ring width of $RW = 850$ nm and a pulley waveguide width of $W = 460$ nm coupled at a gap $G = 600$ nm over a length of $L_c = 17$ μm . The microcomb is pumped at 283.435152 THz ± 10 MHz, and the improved waveguide outcoupling relative to the previous section results in the extraction of a full octave with two harmonic DWs [Fig. 6a]. By injecting the reference pump at the long wavelength DW, 90 modes away from the main pump at 193.510599 THz ± 10 MHz, we observe an increase of approximately 8 dB in the short DW with only 1.5 mW of on-chip reference power [Fig. 6b]. This increase in DW power depends on both the reference pump power and frequency, consistent with LLE simulations (see Supplementary S6). The former is directly related to the self-balancing effect, while the latter is associated with the modification of the repetition rate, as demonstrated in Fig. 6c where we optimize the phase-matching of the azimuthal component at the short DW. By further increasing the reference pump power, it is possible to tune the short DW comb line due to a larger synchronization bandwidth and a greater excursion in the repetition rate variation (see Supplementary S6). Thanks to the reference pump capturing a comb tooth, one can split it before injecting a portion into the microcomb and doubling a portion in a periodically-poled lithium niobate waveguide, where a stage of amplification is needed due to the poor SHG efficiency of 25 %/W. This amplification stage could be removed in a clockwork architecture by harnessing the high conversion efficiency of $\chi^{(2)}$ integrated photonics resonators [47–49], or even potentially the DC-Kerr effect in Si_3N_4 resonators [50]. Due to the high SHG power, an electro-optic comb (see Methods) can be created from the doubled reference to downconvert the expected $\omega_{\text{ceo}} \approx -320 \times 2\pi$ GHz to an easily detectable frequency [Fig. 6d]. As the repetition rate of the DKS in the KIS regime is also changed from

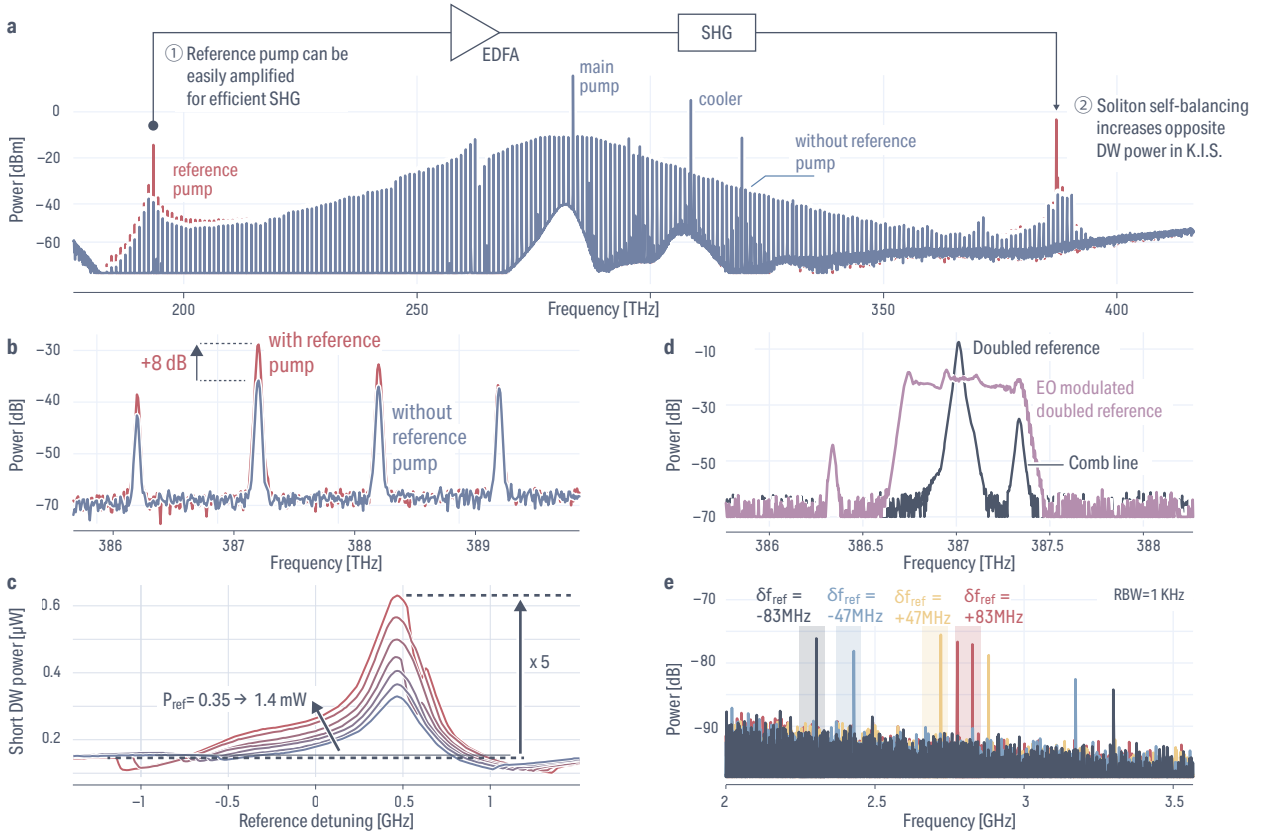


Fig. 6

the reference pump frequency tuning, the CEO frequency will follow a distinct predictable trend. By determining the frequency of each pump using a wavemeter, one can estimate the repetition rate and hence the variation of ω_{ceo} with the reference pump frequency, which aligns well with direct measurement [Fig. 6e]. We note that assuming a KIS bandwidth of 1 GHz allows for about 3 GHz tuning of ω_{ceo} , allowing for some degree of flexibility yet not sufficient for reducing the ω_{ceo} , which can lay between 0 and ± 500 GHz, to a detectable window. To address this, a combination of geometrical tuning (ring radius) and thermal tuning [51] will make ω_{ceo} directly detectable without an EComb apparatus. Nevertheless, our demonstration paves the way for a complete clockwork operation of the microcomb in the KIS regime. In this regime, the stability of the reference laser is automatically divided onto the repetition rate, and the main pump can be independently and coherently locked to the reference pump through improved CEO detection using the KIS-mediated effects.

Discussion — In conclusion, we introduced a new approach for microcomb-based optical frequency division clockworks. Our method uses passive, all-optical Kerr-induced synchronization (KIS), avoiding complex electronic systems. In analogous fashion to mechanical clockworks, passive synchronization is enabled by direct coupling to the reference. In particular, the same resonator and optical nonlinearity enabling DKS generation is used

to achieve synchronization between the DKS and the reference laser. We explored the system’s nonlinear dynamics experimentally and theoretically, demonstrating KIS with milliWatt-level reference laser power compatible with integrated lasers [52].

In contrast to existing self-injection locking approaches where the main pump laser frequency follows the DKS existence condition, here it is the DKS which locks its frequency components to a separate reference pump, providing a direct external control to tune the microcomb parameters. We show that the repetition rate of the DKS can be controlled by adjusting the reference pump frequency, with a tuning set by the frequency division factor. By demonstrating short- and long-term stability division compatible with an optical clock architecture, we show the viability of our clockwork technique. Finally, we demonstrate that KIS enhances CEO frequency detection. Thanks to large SHG power available from the reference pump and the self-balancing effect increasing the short DW, it becomes possible to use an EComb to measure the $f - 2f$ beat note and resolve a CEO frequency in the 300 GHz range. Our work is an important step toward compact optical clocks for fieldable applications in position, navigation, and timing, both by decreasing the power budget and greatly simplifying the architecture for both locking the microcomb to an optical reference and microcomb self-referencing. It also paves the way for future physics investigations that can probe novel DKS

states thanks to the nonlinear connection between CW light and intra-cavity pulses.

-
- [1] Diddams, S. A., Vahala, K. & Udem, T. Optical frequency combs: Coherently uniting the electromagnetic spectrum. *Science* **369**, eaay3676 (2020).
- [2] Fortier, T. & Baumann, E. 20 years of developments in optical frequency comb technology and applications. *Communications Physics* **2**, 153 (2019).
- [3] Ludlow, A. D., Boyd, M. M., Ye, J., Peik, E. & Schmidt, P. O. Optical atomic clocks. *Reviews of Modern Physics* **87**, 637–701 (2015).
- [4] Diddams, S. A. et al. An Optical Clock Based on a Single Trapped $^{199}\text{Hg}^+$ Ion. *Science* **293**, 825–828 (2001).
- [5] Martin, K. W. et al. Compact Optical Atomic Clock Based on a Two-Photon Transition in Rubidium. *Physical Review Applied* **9**, 014019 (2018).
- [6] Bothwell, T. et al. JILA SrI optical lattice clock with uncertainty of. *Metrologia* **56**, 065004 (2019).
- [7] Kippenberg, T. J., Gaeta, A. L., Lipson, M. & Gorodetsky, M. L. Dissipative Kerr solitons in optical microresonators. *Science* **361**, eaan8083 (2018).
- [8] Ma, L.-S. et al. Optical Frequency Synthesis and Comparison with Uncertainty at the 10^{-19} Level. *Science* **303**, 1843–1845 (2004).
- [9] Spencer, D. T. et al. An optical-frequency synthesizer using integrated photonics. *Nature* **557**, 81–85 (2018).
- [10] Coddington, I., Swann, W. C., Nenadovic, L. & Newbury, N. R. Rapid and precise absolute distance measurements at long range. *Nature Photonics* **3**, 351–356 (2009).
- [11] Riemensberger, J. et al. Massively parallel coherent laser ranging using a soliton microcomb. *Nature* **581**, 164–170 (2020).
- [12] Tiesinga, E., Mohr, P. J., Newell, D. B. & Taylor, B. N. CODATA recommended values of the fundamental physical constants: 2018. *Reviews of Modern Physics* **93**, 025010 (2021).
- [13] Holzwarth, R., Zimmermann, M., Udem, T. & Hansch, T. W. Optical clockworks and the measurement of laser frequencies with a mode-locked frequency comb. *IEEE Journal of Quantum Electronics* **37**, 1493–1501 (2001).
- [14] Papp, S. B. et al. Microresonator frequency comb optical clock. *Optica* **1**, 10–14 (2014).
- [15] Newman, Z. L. et al. Architecture for the photonic integration of an optical atomic clock. *Optica* **6**, 680 (2019).
- [16] Drake, T. E. et al. Terahertz-Rate Kerr-Microresonator Optical Clockwork. *Physical Review X* **9**, 031023 (2019).
- [17] Li, Q. et al. Stably accessing octave-spanning microresonator frequency combs in the soliton regime. *Optica* **4**, 193 (2017).
- [18] Okawachi, Y. et al. Octave-spanning frequency comb generation in a silicon nitride chip. *Optics Letters* **36**, 3398–3400 (2011).
- [19] Pfeiffer, M. H. P. et al. Octave-spanning dissipative Kerr soliton frequency combs in Si_3N_4 microresonators. *Optica* **4**, 684–691 (2017).
- [20] Yu, S.-P. et al. Tuning Kerr-Soliton Frequency Combs to Atomic Resonances. *Physical Review Applied* **11**, 044017 (2019).
- [21] Manurkar, P. et al. Fully self-referenced frequency comb consuming 5 watts of electrical power. *OSA Continuum* **1**, 274–282 (2018).
- [22] Shaw, J. K., Fredrick, C. & Diddams, S. A. Versatile digital approach to laser frequency comb stabilization. *OSA Continuum* **2**, 3262–3271 (2019).
- [23] Stern, B., Ji, X., Okawachi, Y., Gaeta, A. L. & Lipson, M. Battery-operated integrated frequency comb generator — Nature. *Nature* **562**, 401–405 (2018).
- [24] Riehle, F. *Frequency Standards: Basics and Applications* (Wiley-VCH, 2004).
- [25] Yang, Q.-F., Yi, X., Yang, K. Y. & Vahala, K. Counter-propagating solitons in microresonators. *Nature Photonics* **11**, 560–564 (2017).
- [26] Wang, Y. et al. Universal mechanism for the binding of temporal cavity solitons. *Optica* **4**, 855 (2017).
- [27] Moille, G. et al. Two-Dimensional Nonlinear Mixing Between a Dissipative Kerr Soliton and Continuous Waves for a Higher-Dimension Frequency Comb. *arXiv* (2023). 2303.10026.
- [28] Moille, G. et al. Ultra-broadband Kerr microcomb through soliton spectral translation. *Nature Communications* **12**, 7275 (2021).
- [29] Qureshi, P. C. et al. Soliton linear-wave scattering in a Kerr microresonator. *Communications Physics* **5**, 1–8 (2022).
- [30] Zhang, S., Silver, J. M., Bi, T. & Del’Haye, P. Spectral extension and synchronization of microcombs in a single microresonator. *Nature Communications* **11**, 6384 (2020).
- [31] Lu, Z. et al. Synthesized soliton crystals. *Nature Communications* **12**, 3179 (2021).
- [32] Taheri, H., Matsko, A. B., Maleki, L. & Sacha, K. All-optical dissipative discrete time crystals. *Nature Communications* **13**, 848 (2022).
- [33] Couillet, P., Gilli, J. M., Monticelli, M. & Vandenberghe, N. A damped pendulum forced with a constant torque. *American Journal of Physics* **73**, 1122–1128 (2005).
- [34] Todd, C. et al. Dynamics of temporal Kerr cavity solitons in the presence of rapid parameter inhomogeneities: From bichromatic driving to third-order dispersion. *Physical Review A* **107**, 013506 (2023).
- [35] Jang, J. K., Erkintalo, M., Coen, S. & Murdoch, S. G. Temporal tweezing of light through the trapping and manipulation of temporal cavity solitons — Nature Communications. *Nature Communications* **6**, 7370 (2015).
- [36] Englebert, N. et al. Bloch oscillations of coherently driven dissipative solitons in a synthetic dimension. *Nature Physics* **19**, 1014–1021 (2023).
- [37] Zhang, S. et al. Sub-milliwatt-level microresonator solitons with extended access range using an auxiliary laser. *Optica* **6**, 206 (2019).
- [38] Zhou, H. et al. Soliton bursts and deterministic dissipative Kerr soliton generation in auxiliary-assisted microcavities. *Light: Science & Applications* **8**, 50 (2019).
- [39] Appleton, E. V. The automatic synchronization of triode OSCillators. *Proc. Cambridge Phil. Soc.* **21** (1922).
- [40] Taheri, H., Matsko, A. B. & Maleki, L. Optical lattice trap for Kerr solitons. *The European Physical Journal D* **71** (2017).

- [41] Moille, G., Li, Q., Xiyuan, L. & Srinivasan, K. pyLLE: A Fast and User Friendly Lugiato-Lefever Equation Solver. Journal of Research of the National Institute of Standards and Technology **124**, 124012 (2019).
- [42] Shen, B. et al. Integrated turnkey soliton microcombs. Nature **582**, 365–369 (2020).
- [43] Voloshin, A. S. et al. Dynamics of soliton self-injection locking in optical microresonators. Nature Communications **12**, 235 (2021).
- [44] Liehl, A. et al. Broadband analysis and self-control of spectral fluctuations in a passively phase-stable Er-doped fiber frequency comb. Physical Review A **101**, 023801 (2020).
- [45] Certain commercial products or names are identified to foster understanding. Such identification does not constitute recommendation or endorsement by the National Institute of Standards and Technology, nor is it intended to imply that the products or names identified are necessarily the best available for the purpose.
- [46] Friederich, F. et al. Phase-locking of the beat signal of two distributed-feedback diode lasers to oscillators working in the MHz to THz range. Optics Express **18**, 8621–8629 (2010).
- [47] Chang, L. et al. Strong frequency conversion in heterogeneously integrated GaAs resonators. APL Photonics **4**, 036103 (2019).
- [48] Chen, J.-Y. et al. Efficient Frequency Doubling with Active Stabilization on Chip. Laser & Photonics Reviews **15**, 2100091 (2021).
- [49] Lu, J., Li, M., Zou, C.-L., Sayem, A. A. & Tang, H. X. Toward 1% single-photon anharmonicity with periodically poled lithium niobate microring resonators. Optica **7**, 1654–1659 (2020).
- [50] Lu, X., Moille, G., Rao, A., Westly, D. A. & Srinivasan, K. Efficient photo-induced second harmonic generation in silicon nitride photonics. Nat. Photon. **15**, 131–136 (2021).
- [51] Moille, G. et al. Integrated buried heaters for efficient spectral control of air-clad microresonator frequency combs. APL Photonics **7**, 126104 (2022).
- [52] Xiang, C. et al. Laser soliton microcombs heterogeneously integrated on silicon. Science **373**, 99–103 (2021).
- [53] Stone, J. R. & Papp, S. B. Harnessing Dispersion in Soliton Microcombs to Mitigate Thermal Noise. Physical Review Letters **125**, 153901 (2020).

Fig. 1 – Clockwork concept – **a** Mechanical Shortt’s clock concept (left) and its optical counterpart. This scheme, which is the current state-of-the-art approach, links a reference laser stabilized to atomic transition f_{ref} with a microcomb tooth (typically at the dispersive wave f_{DW}) to reduce frequency to the microcomb rate f_{rep} . The active feedback increases power budget and complexity, resulting in chip-scale integration challenges. **b** Mechanical Huygens’ clock concept (left) and equivalent optical clockwork. This scheme corresponds to the concept of passive Kerr-induced synchronization (KIS) between the reference and the comb, which we study in this work. In the mechanical clock, the coupling between the two pendulums is lossy and results in poor long term stability. In the optical regime, the coupling can be provided by the lossless optical Kerr nonlinearity. The coupling link between the DKS and the reference laser created by injecting the latter directly into the DKS microresonator enables passive synchronization for a significantly simplified optical clockwork. In addition to passive synchronization, we show in this work that the KIS regime also dramatically improves the detection and locking of the CEO frequency.

Fig. 2 – Concept of phase locking for Kerr-induced synchronization (KIS) – **a** DKS circulating in a resonator where the envelope travels at the group velocity while the fast oscillations travel at a distinct phase velocity, resulting in a non-zero carrier envelope offset. A second, reference pump laser can also be injected into the DKS resonator. **b** In the unsynchronized case, the phase velocities of the reference and pump components of the MDKS are different, yielding a constant phase slip in time, and hence an offset in CEO observable in the comb spectrum. **c** In the KIS case, there is no temporal phase slip between the components, and thus the MDKS becomes a single DKS. Consequently, no CEO frequency offset is observable as the reference pump has captured a comb tooth.

Fig. 3 – Experimental demonstration of synchronization. – **a** Experimental (open circles) vs. simulated (dashed line) dispersion of the microring resonator highlights an accessible dispersive wave (DW) at $\mu = -92$ (≈ 194 THz). Another high-frequency DW is inaccessible due to pulley-coupling optimizing the main and the reference pump coupling. **b** OFC obtained while pumping at 284 THz with a cooler at 308 THz for thermal stability, and a reference pump near 194 THz. The different regimes of the DKS with different detunings of the reference at $\mu = -91$ are highlighted. **c** Recording of the CEO frequency mismatch Ω (y axis) with the reference pump detuning $\delta\omega_{\text{ref}}$ (x axis). The absence of a beat in the central region is a signature of the synchronization. The experimental data (left) are reproduced accurately by the LLE (right). **d** Zoom-in around the DW mode, exhibiting lower comb tooth power the further from $\mu = -92$ the azimuthal component is. **e** The KIS bandwidth depends on both the reference pump and azimuthal mode number power. As expected by the Adler equation, we observe a decrease of the bandwidth for lower comb tooth power. The reduced maximum power arises from decoupling from mechanical relaxation over time.

Fig. 4 – Control of the DKS repetition rate from the reference pump alone – **a** Concept of repetition rate tuning. In the KIS state, the reference pump is a comb tooth, and thus its tuning stretches or compresses the OFC, resulting in a shift of the repetition rate. **b** LLE simulation of the repetition rate shift with the reference pump detuning. The slope in the synchronization window is the expected frequency division factor $\mu_s = -89$ (top). We verify the change in slope when the reference pump is tuned to different azimuthal mode numbers (bottom). **c** Optical frequency comb under study, similar to Fig. 3. We use the electro-optic comb apparatus to translate two comb teeth in a detectable bandwidth (inset). The teal comb is in the KIS regime; dark blue is without the reference pump. **d** Experimental measurement of the repetition rate change with the reference pump detuning. The slope in the synchronization window respects the division factor μ_s for different probed azimuthal mode numbers, in accordance with simulation predictions.

Fig. 5 – Validation of the clockwork under passive synchronization – **a** Electrical spectrum analyzer measurement of the DKS repetition rate under different conditions, including without reference pump synchronization (left), synchronization but with the main and reference unlocked (middle), and synchronized with the main and reference pumps locked to a fiber frequency comb. The frequency axes have been referenced to the actual DKS repetition rate frequency. The power is normalized to 1 mW. **b** Frequency counter trace (gate time of 10 ms) of the repetition rate in a synchronized state with lasers locked to the fiber comb, highlighting a standard deviation of about 12 Hz (red dashed lines), for an average repetition rate of 997,387,327,768 Hz. **c** Repetition rate phase noise comparison: unsynchronized single pump (red), KIS regime (green) with a locked main pump. The free-running reference pump’s phase noise divided by the number of modes between pinned teeth (blue) matches the repetition rate noise, indicating frequency division. The main pump’s scaled phase noise (grey) is negligible. Power is referenced to that of the carrier, i.e., dBc/Hz. **d** Long-term of the repetition rate’s stability in the KIS regime (green) compared to the fiber comb (dark blue). The $1/\tau$ trend at long averaging time showcases coherent phase locking. Plateau between 1s to 10s are likely due to environmental factors. The schematic represents links between the 10MHz Rb standard, 80MHz fiber comb, and the synchronized DKS rate.

Fig. 6 – Carrier Envelope Detection Improvement: Self-Balancing and Large SHG Power – **a** Experimental microcomb with harmonic DW, synchronized with a 1.5 mW reference pump (red) and without (blue). The CEO measurement is made possible thanks to the large available SHG power from the reference and the increase in short DW power via self-balancing. **b** Increase of the short DW by 8 dB through the self-balancing effect that increases the DW opposite to the reference laser. **c** Experimental measurement of the short DW power dependence with the reference power and detuning using a 800 nm short pass filter and a power meter. The peaks correspond to reference pump tuning the repetition rate of the microcomb into optimal phase matching for the short DW. The power dependence arises from the synchronization condition for which the soliton must balance, hence increasing its radiation into the short DW. **d** Optical spectrum around the SHG of the reference laser with (purple) and without (dark blue) electro-optic modulation to create an electro-optic comb for detecting the >300 GHz CEO frequency. **e** Measurements of the CEO frequency. Tuning the reference pump frequency impacts both ω_{rep} and ω_{ceo} . Different reference frequencies yield varying ω_{ceo} values, consistent with predictions and a 20 MHz uncertainty. Beat notes symmetrically align against the electro-optics modulator’s driving frequency $\omega_{\text{eo}} = 5.6033 \times 2\pi$ GHz.

Methods

LLE simulations – The extended Lugiato Lefever equation model including multiple driving fields can be written as [40]:

$$\begin{aligned} \frac{\partial a(\theta, t)}{\partial t} = & -\frac{\kappa}{2}a + i \sum_{\mu} A(\mu, t) D_{\text{int}}(\mu) e^{i\theta\mu} \quad (2) \\ & + \Delta D_1 \frac{\partial a}{\partial \theta} + i\gamma L |a|^2 a \\ & + i \sum_j \sqrt{\kappa_{\text{ext}} P_j} e^{i\mu_j \theta + i(D_{\text{int}}(\mu_j) + \delta\omega_j)t} \end{aligned}$$

with $a(\theta, t) = \sum_{\mu} A(\mu, t) e^{i\theta\mu}$, κ and κ_{ext} the total and external losses, P_j the power of each driving field j , $D_{\text{int}}(\mu_j)$ the integrated dispersion at the azimuthal mode j , $\gamma = \omega \frac{n_2}{A_{\text{eff}}}$ the effective nonlinearity with n_2 the material nonlinearity and A_{eff} the effective mode area, $L = 2\pi R$ the resonator round trip length, and ΔD_1 the mismatch between the linear free spectral range at the pump (*i.e.* from which D_{int} is defined) and the soliton repetition rate. In our system, we are in the presence of two driving fields, the main pump at $\mu = 0$ and the reference at μ_s . To obtain the optical frequency comb that is observed in experiment the following protocol is observed, similar to the one presented in ref [27]:

1. For each reference detuning $\delta\omega_{\text{ref}}$, find ΔD_1 such that the soliton position in θ is invariant with t
2. Solve the LLE and sample the soliton at every round trip time to effectively emulate the periodic extraction by the bus waveguide
3. Reconstruct the pulse train by concatenating every sampled soliton to obtain $a_{\text{wg}}(t)$
4. Fourier transform the pulse train to reconstruct the OFC and obtain $A_{\text{wg}}(\omega)$
5. Recast the frequency comb into a two dimensional system $A_{\text{wg}}(\mu, \Omega)$ by resizing $A_{\text{wg}}(\omega)$ by the repetition rate sampling size, thus any power component within $[-\omega_{\text{rep}}/2; +\omega_{\text{rep}}/2]$ around a given comb tooth μ of the DKS
6. Integrate $A_{\text{wg}}(\mu, \Omega)$ along μ to obtain $S(\Omega)$, which is equivalent to the experimental measurement of the beat note arising from the CEO frequency shift.
7. Repeat for every $\delta\omega_{\text{ref}}$ to create the plot presented in Fig. 3c.

In order to retrieve the dynamics presented in Fig. 4, there is no need to obtain $S(\Omega)$ but rather it is about finding ΔD_1 . If one assumes a very slow variation of $\delta\omega_{\text{ref}}$, we can make the approximation that $\delta\omega_{\text{ref}}$ is constant in between t and $t + \delta t$. One can then extract the drift of the soliton within this time window and obtain ΔD_1 .

Electro-optic comb apparatus for ω_{rep} detection– For an OFC to span over an octave in an on-chip format, the repetition rate must be high, here about 997 GHz, to minimize the number of comb teeth needed to span the octave and reduce the pump power needed. We use

an electro-optic comb (EOcomb) apparatus [53] made of three cascaded electro-optic (EO) phase modulators driven at $f_{\text{EO}} = 17.47$ GHz to measure the DKS repetition rate by modulating two of its adjacent OFC comb teeth. The phase modulation of the DKS OFC teeth forms an EO comb spanning over 1 THz with $N_{\text{EO}} = 57$ EO teeth, which, where they overlap, allows us to record their beat note and infer the DKS repetition rate $f_{\text{rep}} = N_{\text{EO}} f_{\text{EO}} \pm f_{\text{beat}}$ [Fig. 4c].

Electro-optic comb apparatus for ω_{CEO} detection– To measure the CEO frequency in Fig. 6, we used two cascaded electro-optic modulators driven at a frequency $\omega_{\text{EO}} = 5.6033 \times 2\pi$ GHz. This, combined with the increased power of the high frequency DW through the self-balancing effect, enables efficient detection of the CEO using a 10 GHz photodiode [Fig. 6d]. Thanks to the KIS regime, DKS repetition rate can be estimated by using a wavemeter measurement for each pump, allowing to retrieve the expected CEO frequency.

Phase noise measurement – The single comb line or laser phase noise is measured through a 10 MHz FSR Mach-Zehnder interferometer (see Supplementary S4) with a low noise 125 MHz photodiode and electrical spectrum analyzer. The repetition rate noise in the KIS regime is measured using the EOcomb apparatus and a photodiode with a noise floor of -72 dBc/Hz over its 50 MHz bandwidth, and characterized using a phase noise analyzer (PNA) referenced to the EOcomb synthesizer. The repetition rate frequency in the unsynchronized case is not stable enough to be measured using the PNA, hence it is derived from the individual comb tooth noise at $\mu = 92$ in the absence of the reference pump (see Supplementary S5) and with a locked main pump using the MZI detection method.

General experimental protocol – For a complete description of the experimental setup, please refer to the Supplementary S2. To measure the CEO offset highlighting the synchronization in Fig. 2, a 6 GHz photodiode measures the comb, with the main pump and the cooler filtered out. For measuring the repetition rate in Fig. 4, we send two adjacent OFC teeth through the EO comb apparatus. We then use a narrow filter to only select the two EO comb teeth that participate in the frequency downconversion repetition rate beat note, which we record with a 50 MHz avalanche photodiode. For the noise measurements presented in Fig. 5, the same type of filtering is used with the 80 MHz fiber comb beating against a single DKS OFC tooth.

Acknowledgments

The photonic chips were fabricated by Ligentec SA. The authors acknowledge partial funding support from the AFRL Space Vehicles Directorate, the DARPA APhi program, and the NIST-on-a-chip program. C.M. acknowledges support from the Air Force Office of Scientific Research (AFOSR grant FA9550-20-1-0357). We thank Pradyoth Shandilya, Marcelo Davanço, and

Vladimir Aksyuk for insightful feedback. We thank Michael Highman and Matt Cich from Toptica Photonics for loan of the fiber comb.

Author Contributions

G.M. led the project, designed the resonators, performed the measurements and simulations, and developed the Adler equation model. J. S. helped with the metrology analysis. M. C. developed the electro-optic comb apparatus. R. S. and U. A. J. helped with the second harmonic characterization. C. M. contributed in the understanding of the physical phenomenon. K. S. helped with guiding the project and in data analysis. G. M. and K. S. wrote the manuscript, with input from all authors.

All the authors contributed and discussed the content of this manuscript.

Competing Interests

The authors declare no competing interests.

Data availability

The data that supports the plots within this paper and other findings of this study are available from the corresponding authors upon reasonable request.

Code availability

The simulation code is available from the authors through the pyLLE package available online [41], using the inputs and parameters presented in this work.

Supplementary material of “Kerr-Induced Synchronization of a Cavity Soliton to an Optical Reference”

Grégory Moille,^{1,2,*} Jordan Stone,^{1,2} Michal Chojnacky,^{1,3} Rahul Shrestha,¹ Usman A. Javid,^{1,2} Curtis Menyuk,⁴ and Kartik Srinivasan^{1,2,†}

¹Joint Quantum Institute, NIST/University of Maryland, College Park, USA

²Microsystems and Nanotechnology Division, National Institute of Standards and Technology, Gaithersburg, USA

³Sensor Science Division, National Institute of Standards and Technology, Gaithersburg, USA

⁴University of Maryland at Baltimore County, Baltimore, MD, USA

(Dated: September 3, 2023)

S-1. Adler equation for the Multi-Color DKS (MDKS)

We are seeking to find the equation of motion of the system, in particular the equation describing the evolution in time of the phase difference between the reference pump laser φ_{ref} at azimuthal mode μ_s (defined relative to the main pump at $\mu = 0$) and the corresponding DKS azimuthal component A_{μ_s} with the phase $\varphi_{\text{dks}}(\mu_s)$. We know that the carrier envelope offset frequency arises from the phase velocity, such that $\omega_{\text{ceo}} = \partial\varphi/\partial t$. We are assuming that the pulse that is generated by the reference laser is locked to the pulse that is generated by the pump laser to form a single MDKS that propagates with a single group velocity. However, each component of the MDKS will in general have its own phase velocity, hence its own CEO frequency $\omega_{\text{ceo}}^{(\text{ref})}$ and $\omega_{\text{ceo}}^{(\text{dks})}$ for the reference and main component of the MDKS respectively. This phase velocity difference is given by:

$$\begin{aligned} \frac{\partial\Phi}{\partial t} &= \frac{\partial\varphi_{\text{ref}}}{\partial t} - \frac{\partial\varphi_{\text{dks}}(\mu_s)}{\partial t} \\ &= \omega_{\text{ceo}}^{(\text{ref})} - \omega_{\text{ceo}}^{(\text{dks})} \\ &= \omega_{\text{ref}} - \omega_{\text{dks}}(\mu_s) \\ &= \omega_{\text{cav}}(\mu_s) + \delta\omega_{\text{ref}} - (\omega_0 + \mu_s\omega_{\text{rep}}) \end{aligned} \quad (\text{S.1})$$

with φ_{ref} and $\varphi_{\text{dks}}(\mu_s)$ the relative phase of the reference pump and its closest DKS azimuthal component respectively, $\omega_{\text{ceo}}^{(X)}$ being the CEO frequency relative to the DKS ($X = \text{dks}$) or the reference pump ($X = \text{ref}$), ω_{ref} is the frequency of the reference pump which is offset from the cavity resonance $\omega_{\text{cav}}(\mu_s)$ by a detuning $\Delta\omega_{\text{ref}}$, and $\omega_{\text{dks}}(\mu_s) = \omega_0 + \mu_s\omega_{\text{rep}}$ is the frequency of the closest comb tooth from the reference pump frequency with ω_{rep} being the repetition rate of the DKS and ω_0 being the main pump frequency. $\frac{\partial\Phi}{\partial t}$ represents the repetition rate in the second dimension of the 2D comb reported in ref. [1].

Additional differentiation of Eq. (S.1) provides a direct link between the phase mismatch Φ and ω_{rep} :

$$\frac{\partial^2\Phi}{\partial t^2} = -\mu_s \frac{\partial\omega_{\text{rep}}}{\partial t} \quad (\text{S.2})$$

We now suppose that in the resonator angular coordinate θ there is a short-duration pulse whose central angle $\bar{\theta}$ is well-defined and rotates at a constant angular velocity with a fixed shape. Therefore, we have:

$$E_{\text{dks}}\bar{\theta} = \int_{-\pi}^{\pi} \theta |a(\theta, t)|^2 \frac{d\theta}{2\pi} \quad (\text{S.3})$$

where $a(\theta, t)$ satisfies the modified LLE equation presented in Eq 2 in the Methods. The quantity E_{dks} is given by $\int \frac{d\theta}{2\pi} |a(\theta, t)|^2$ and represent the DKS energy, so that $\bar{\theta}$ is the pulse averaged central angle of the pulse. We then have

$$E_{\text{dks}} \frac{d\bar{\theta}}{dt} = \frac{d}{dt} \int_{-\pi}^{\pi} \theta |a(\theta, t)|^2 \frac{d\theta}{2\pi} = \int_{-\pi}^{\pi} \theta \left[a \frac{\partial a^*}{\partial t} + a^* \frac{\partial a}{\partial t} \right] \frac{d\theta}{2\pi} \quad (\text{S.4})$$

* gregory.moille@nist.gov

† kartik.srinivasan@nist.gov

We must first assume that the loss and gain terms make a negligible contribution to the momentum. This assumption implies:

$$0 \approx \int_{-\pi}^{\pi} \theta |a(\theta, t)|^2 \frac{d\theta}{2\pi} = \int_{-\pi}^{\pi} \theta [F a^* + F^* a - \kappa |a|^2] \frac{d\theta}{2\pi} \quad (\text{S.5})$$

with F being the main driving force in Eq 2 in the Methods and we assume the reference pump is negligible before the main pump power, which is the case in our experiment. The assumption that the loss and gain terms are negligible is reasonable since the magnitude of these terms is small. There is, however, no expectation that it is exactly zero. Otherwise, the Kerr effect terms cancel out, so we can thus focus on the linear contribution, which is the dominant contribution. It is useful now to work in the mode number domain. We write:

$$A(\mu, t) = \int_{-\pi}^{\pi} \frac{d\theta}{2\pi} a(\theta, t) e^{-i\mu\theta}, \quad a(\theta, t) = \sum_{\mu} A(\mu, t) e^{i\mu\theta} \quad (\text{S.6})$$

We then have under the same approximations:

$$\frac{dA(\mu)}{dt} \equiv i\omega_{\text{cav}}(\mu) A(\mu) \quad (\text{S.7})$$

with $\omega_{\text{cav}}(\mu)$ the azimuthal component optical frequencies on resonance. Using Eq. (S.7) and injecting it in Eq. (S.4), accounting only for the linear terms, integrating by parts, and noting that only the term $\mu = 0$ survive the integration, we obtain:

$$E_{\text{dks}} \frac{d\bar{\theta}}{dt} = - \sum_{\mu} \omega'_{\text{cav}}(\mu) A(\mu) A^*(\mu) \quad (\text{S.8})$$

with $\omega'_{\text{cav}}(\mu) = \frac{d\omega_{\text{cav}}(\mu)}{d\mu}$. It should be noted that we are assuming that A_{μ} and $\omega_{\text{cav}}(\mu)$ are both continuous functions of μ with continuous derivatives, and thus assuming a resonator without mode coupling to different propagation directions (*i.e.* backscattering) or mode families (*i.e.* avoided mode crossing).

The dispersion can be accounted in different fashions, either through a Taylor expansion assuming mode-independent coefficients or assuming a mode-dependent free spectral range such that $\omega'_{\mu} = \frac{d\omega_{\mu}}{d\mu} = D_1(\mu)$. Noting that in the cavity referential the temporal variation of the the pulse averaged central angle $\frac{\partial \bar{\theta}}{\partial t}$ translates directly into the repetition rate ω_{rep} , we can write :

$$\omega_{\text{rep}} = - \frac{1}{E_{\text{DKS}}} \sum_{\mu} D_1(\mu) A(\mu) A^*(\mu) \quad (\text{S.9})$$

Taking the time derivative of this equation, we obtain:

$$\frac{\partial \omega_{\text{rep}}}{\partial t} = - \frac{1}{E_{\text{DKS}}} \sum_{\mu} D_1(\mu) \left(\frac{\partial A(\mu)}{\partial t} A^*(\mu) + A(\mu) \frac{\partial A^*(\mu)}{\partial t} \right) \quad (\text{S.10})$$

We can write the coupled mode theory equation for each azimuthal mode component $A(\mu)$ accounting for the Kerr nonlinearity as:

$$\frac{\partial A(\mu)}{\partial t} = \left(-\frac{\kappa}{2} + i\omega_{\text{cav}}(\mu) \right) A(\mu) + i\gamma L \sum_{\alpha, \beta} A(\alpha) A^*(\beta) A(\alpha - \beta + \mu) - i\delta(\mu_0) \sqrt{\kappa_{\text{ext}} P_{\text{main}}} e^{i\omega_0 t} - i\delta(\mu_s) \sqrt{\kappa_{\text{ext}} P_{\text{ref}}} e^{i\omega_{\text{ref}} t} \quad (\text{S.11})$$

Here, $\omega_{\text{cav}}(\mu)$ are the resonance frequencies of the modes μ normalized to the pump mode, $\gamma = \omega n_2 / A_{\text{eff}}$ is the effective nonlinear coefficient, with $n_2 = 2.4 \times 10^{-15} \text{ cm}^2 \cdot \text{W}^{-1}$, which we assume constant for simplification (yet given the comb bandwidth it should not be), L is the circumference of the resonator, κ_{ext} is the coupling rate and κ the total loss rate, P_{main} and P_{ref} are the main and reference pump laser power, μ_s is the azimuthal mode at which the reference laser is situated, and $\delta(x)$ is the Kronecker delta function such that $\delta(\mu = x) = 1$ and $\delta(\mu \neq x) = 0$. We note that μ_0 is the

main pumped mode, which is null here per normalization, yet we explicitly label it here to avoid confusion with a simple zero.

Plugging Eq. (S.11) into Eq. (S.10), several things can be simplified. First, we can note that all linear imaginary components of Eq. (S.11) cancel each other out for each μ , and only the terms where the pumps are presents need to be kept. In addition, we can note that the relative phase between the main pump and its corresponding phase is fixed. Thus we obtain the following equation for the temporal derivative of the repetition rate:

$$-\frac{\partial\omega_{\text{rep}}}{\partial t} = \kappa D_1(\mu_s) K_s \sin\left[(\varphi_{\text{ref}} - \varphi_{\text{dks}}(\mu_s))t\right] + \kappa D_1(\mu_0) K_0 - \kappa D_1(\mu_0) K_{NL} - \kappa\omega_{\text{rep}} \quad (\text{S.12})$$

Here, we note that the sin function appears because of $-i(c - c^*) = 2\mathcal{I}c$. The following parameters are defined:

$$K_s = \frac{2|A(\mu_s)|}{E_{\text{DKS}}} \sqrt{\frac{P_{\text{ref}}\kappa_{\text{ext}}}{\kappa^2}} \quad K_{NL} = \frac{\gamma L}{\kappa D_1(\mu_0) E_{\text{DKS}}} \sum_{\mu} D_1(\mu) \left(A^*(\mu) \sum_{\alpha, \beta} A(\alpha) A^*(\beta) A(\alpha - \beta + \mu) - c.c \right)$$

$$K_0 = \frac{2|A(\mu_0)|}{E_{\text{DKS}}} \sqrt{\frac{P_{\text{main}}\kappa_{\text{ext}}}{\kappa^2}}$$

Using Eq. (S.2) and Eq. (S.10), we arrive at:

$$\frac{1}{\kappa} \frac{\partial^2 \Phi}{\partial t^2} = -\mu_s D_1(\mu_s) K_s \sin(\Phi) + \mu_s D_1(\mu_0) K_{NL} + \mu_s \omega_{\text{rep}} \quad (\text{S.13})$$

Using Eq. (S.1), we can replace ω_{rep} to obtain the extended Adler equation which describes the phase locking of the soliton to the reference laser:

$$-\frac{1}{\kappa} \frac{\partial^2 \Phi}{\partial t^2} + \frac{\partial \Phi}{\partial t} = -\mu_s D_1(\mu_s) K_s \sin(\Phi) + \mu_s D_1(\mu_0) K_{NL} - \mu_s D_1(\mu_0) K_0 + \delta\omega_{\text{ref}} - \omega_0 + \omega_{\text{cav}}(\mu_s) \quad (\text{S.14})$$

We can recall:

$$\omega_{\text{cav}}(\mu_s) - \omega_0 = D_{\text{int}}(\mu_s) + \mu_s D_1(\mu_0)$$

Leading to

$$-\frac{1}{\kappa} \frac{\partial^2 \Phi}{\partial t^2} - \frac{\partial \Phi}{\partial t} = D_{\text{int}}(\mu_s) + \Delta - \mathcal{T} \sin(\Phi) \quad (\text{S.15})$$

This results in the equation of motion of a damped pendulum under constant torque driving [2], with the effective detuning $\Delta = \delta\omega_{\text{ref}} + \mu_s D_1(\mu_0)(1 + K_{NL} - K_0)$ along with $D_{\text{int}}(\mu_s)$ associated to the damping of the effective pendulum system, and $\mathcal{T} = D_1(\mu_s) K_s \mu_s$ the effective ‘‘natural’’ torque of the system (*i.e.* the mass, cord length and gravity acceleration product). For the synchronization to occur, the right hand-side of the equation needs to cancel out. This leads to a condition on the integrated dispersion at the reference pumped mode, which needs to be minimized or needs to be compensated for by the reference pump detuning. As $\delta\omega_{\text{ref}}$ is limited, this imposes a hard limit on which mode can be used. Hence, sending the reference laser at the modes where the DW(s) occur allows one to minimize $D_{\text{int}}(\mu_s)$ and reach a synchronization regime.

From the above, we can extract the locking bandwidth for which the reference laser can be tuned while maintaining synchronization, around a center frequency yet to be determined, as follows:

$$\Delta\omega_{\text{lock}} = 2\mathcal{T} = 4D_1(\mu_s)\mu_s \frac{|A(\mu_s)|}{E_{\text{DKS}}} \sqrt{\frac{P_{\text{ref}}\kappa_{\text{ext}}}{\kappa^2}} \quad (\text{S.16})$$

To give some more insight about the typical values associated with KIS of the DKS to the reference pump laser in our system, we extract the following parameters from the LLE and experiment:

Parameter	Values
$ A(\mu_0) $	$3 \times 10^2 \text{ J}^{1/2}$
$ A(\mu_s) $	$1 \times 10^{-2} \text{ J}^{1/2}$
E_{DKS}	$1 \times 10^{-3} \text{ J}$
κ_{ext}	$2\pi \times 80 \text{ MHz}$
κ	$2\pi \times 150 \text{ MHz}$
μ_s	92
P_{main}	150 mW
P_{ref}	1 mW
K_{μ_s}	4×10^{-6}
K_0	1.4×10^{-5}
$D_1(\mu_0)$	$2\pi \times 1 \text{ THz}$
$\mu_s D_1(\mu_0) K_0$	$2\pi \times 1.26 \text{ GHz}$
$\mu_s D_1(\mu_0) K_{NL}$	$2\pi \times 100 \text{ MHz}$
\mathcal{T}	$2\pi \times 365 \text{ MHz}$
$\Delta\omega_{\text{lock}}$	$2\pi \times 730 \text{ MHz}$

Finally, we can determine how a small change in the reference pump detuning $\delta\omega_{\text{ref}}$, which we call $d\delta\omega_{\text{ref}}$, is related to a small change in ω_{rep} , which we call $d\omega_{\text{rep}}$, simply by differentiating Eq. (S.1), noting that in the synchronization regime $\partial\Phi/\partial t = 0$, and assuming the frequency of resonance and the pump are fixed (as in the experiment). This yields:

$$d\delta\omega_{\text{ref}} = \mu_s d\omega_{\text{rep}} \quad (\text{S.17})$$

Hence, any variation of the reference pump detuning is frequency divided onto the repetition rate with a factor defined by the reference pump mode number μ_s (assuming the main pump remains fixed), similar to the experimental demonstrations in Fig. 4

S-2. Complete experimental setup

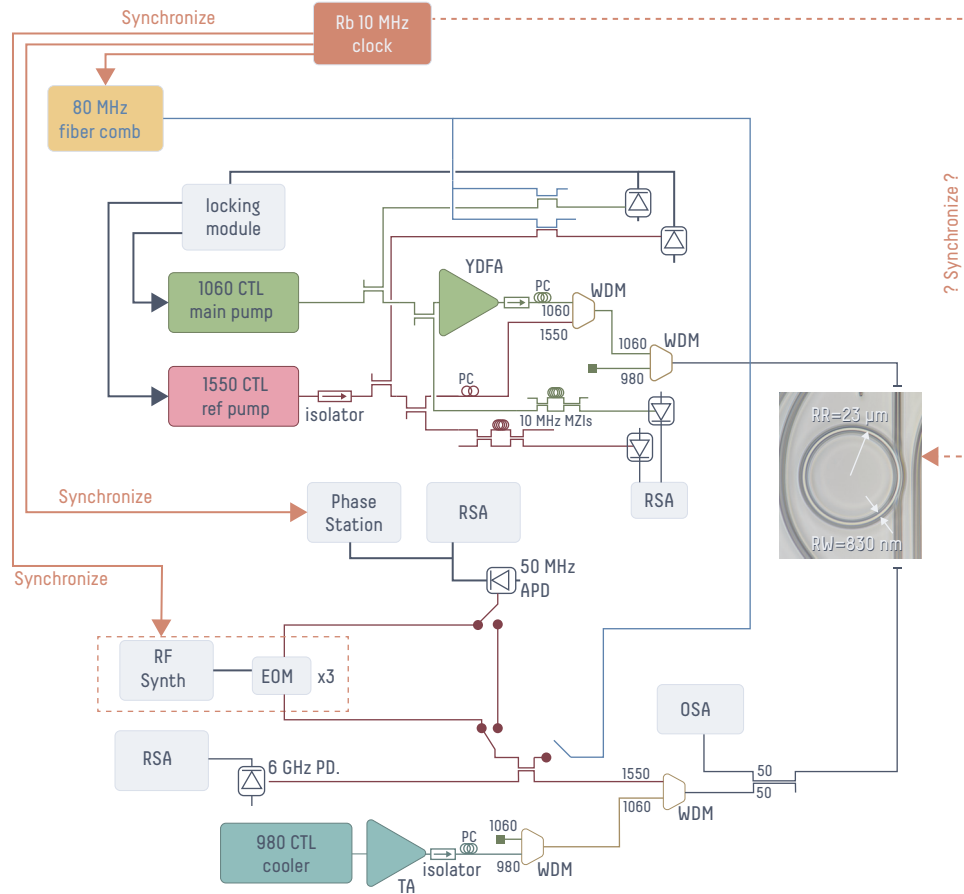


Fig. S1 – Complete experimental setup. EOM: Electro-optical modulator; RSA: real time electrical spectrum analyzer; OSA: optical spectrum analyzer; WDM: wavelength demultiplexer; CTL : continuous tunable laser; MZI: Mach-Zehnder interferometer; APD: avalanche photodiode; PC: polarization controller; YDFA: Ytterbium-doped fiber amplifier; TA: tapered amplifier

The complete experimental setup is presented in Fig. S1. Although it seems quite complex at first, most of the components are dedicated to characterizing the synchronization state, which in an application system would not have to be used. Three CTLs are used, a main pump from a 1060 nm CTL, a reference laser from a 1550 nm CTL, and a cooler pump from a 980 nm CTL. Only the reference laser is not amplified, as the synchronization does not require high power to be obtained. The polarization is set for each laser, transverse electric for the reference and main pump, and transverse magnetic for the cooler to avoid spurious nonlinear mixing in the ring. The reference and the main pump have a small amount of their power tapped for them to be locked to the 80 MHz Toptica fiber comb and sent to the MZIs for frequency noise characterization. The different lasers are combined using wavelength demultiplexers (WDMs). The cooler is filtered out after the chip to avoid high 980 nm power going upstream toward the main and reference pump.

To characterize the DKS OFC, a portion of the light at the output of the chip is sent to the optical spectrum analyzer. The other part of the light exiting the chip is sent to different WDMs for filtering before being sent to different instruments. The CEO offset measurement presented in Fig. 2 is obtained by sending the 1550 nm WDM filtered light to a 6 GHz photodiode, with the output analyzed with an electrical spectrum analyzer for each reference detuning. To obtain either the repetition rate presented in Fig. 4 or the repetition rate noise in Fig. 5, we tap a portion of the light going to the 6 GHz photodiode to either go through the EO comb apparatus or beat directly against the fiber comb. Then a narrow bandpass filter is used to select only the frequency components playing a role in the beating, which is then detected using a 50 MHz avalanche photodiode and processed either with the electrical spectrum analyzer or the phase noise analyzer.

S-3. Arnold tongue bistability

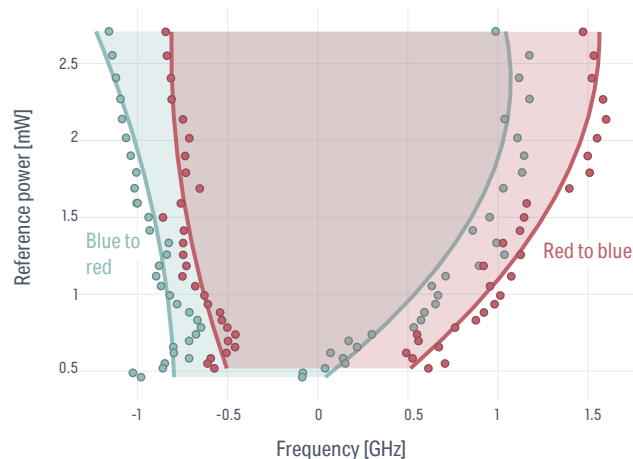


Fig. S2 – Arnold tongue hysteresis exhibiting a different behavior if probed from red to blue detuning or from blue to red. Although thermal bistability could exist, the very low reference laser power – especially below 1 mW – suggests that it alone is unlikely to explain the observed hysteresis. The zero is determined in both cases by a fixed frequency that is measured accurately (< 30 MHz uncertainty) with a wavemeter.

The measurements shown in Fig. 2 of the synchronization bandwidth with reference power are analogous to the well-known Arnold tongue. The experiments presented in the main text are performed with reference laser detuning from red (frequency) to blue (lower frequency). With the on-chip power of the reference below 3 mW, little thermal bistability would be expected, and no bistability at all should be expected with power below 1 mW. However, performing the Arnold tongue characterization with blue-to-red or red-to-blue tuning exhibit a hysteresis, a signature of bistability. The zero frequency of the reference detuning is the same for both scanning directions and is determined with a wavemeter with an accuracy of about 30 MHz, better than the measured hysteresis bandwidth of about 500 MHz.

S-4. Frequency noise estimation from Mach-Zehnder transmission measurement

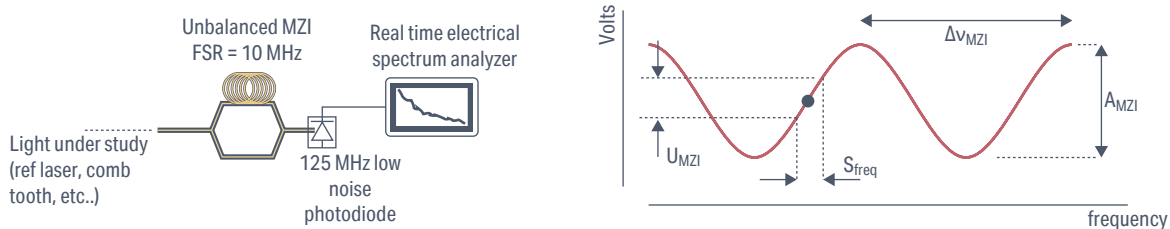


Fig. S3 – **a** Schematic of the MZI used to measure the frequency noise of the laser. **b** Concept to retrieve the frequency noise from the noise measurement of the light set at the quadrature point of the MZIs, converting the frequency noise into voltage noise which can be observed through an electrical spectrum analyzer.

In order to measure the frequency noise of the reference laser as shown in Fig. 5, or of a single comb tooth as described in Section S-5, we used an imbalanced fiber Mach-Zehnder interferometer with a free spectral range of 10 MHz. Working at the quadrature point allows us to convert the frequency noise of the light under study into a voltage noise which can then be observed and processed using a spectrum analyzer (RSA). To retrieve the frequency noise from the RSA, the following algebra is used:

$$S_\nu = \left[\frac{\Delta V_{\text{MZI}}}{\pi} \sin^{-1} \left(\frac{U_{\text{MZI}}}{A_{\text{mzi}}} \right) \right]^2 \quad [\text{Hz}^2/\text{Hz}] \quad (\text{S.18})$$

with $U_{\text{MZI}} = \sqrt{50 \times 10^{-3} \times 10^{S_{\text{MZI}}/10}}$ the voltage obtained from spectral measurement, where S_{MZI} is the optical power in decibels normalized to 1 mW of the MZI noise at quadrature (i.e., in dBm), the spectrum analyzer impedance is assumed to be 50Ω , A_{mzi} is the amplitude of the sinusoidal modulation with frequency of the MZI, and $\Delta\nu_{\text{MZI}}$ is the free spectral range of the MZI at the frequency of interest [Fig. S3].

To convert the frequency noise to phase noise, we use the following relation:

$$S_\varphi = 10 \log_{10} \left(\frac{S_\nu}{\nu^2} \right) \quad [\text{dBc/Hz}] \quad (\text{S.19})$$

S-5. Single comb tooth noise reduction

The frequency noise of the individual comb teeth of a microcomb OFC grows quadratically with the mode number, mainly since the thermo-refractive noise (TRN) is one of the dominant noise sources in such a compact cavity. However, in the synchronized case, the repetition rate is fixed by the two pinned frequencies: the reference and the CEO frequency (when the CEO is stabilized); or, in our case for the latter, the main pump frequency. To this extent, measuring the frequency noise of a single comb tooth in the different regimes is interesting. From Fig. S4, it is clear that in the unsynchronized case, the noise is relatively high and follows the characteristic TRN profile. When in the synchronized case, each comb line's noise is significantly reduced and follows the noise characteristic of the pinned frequencies.

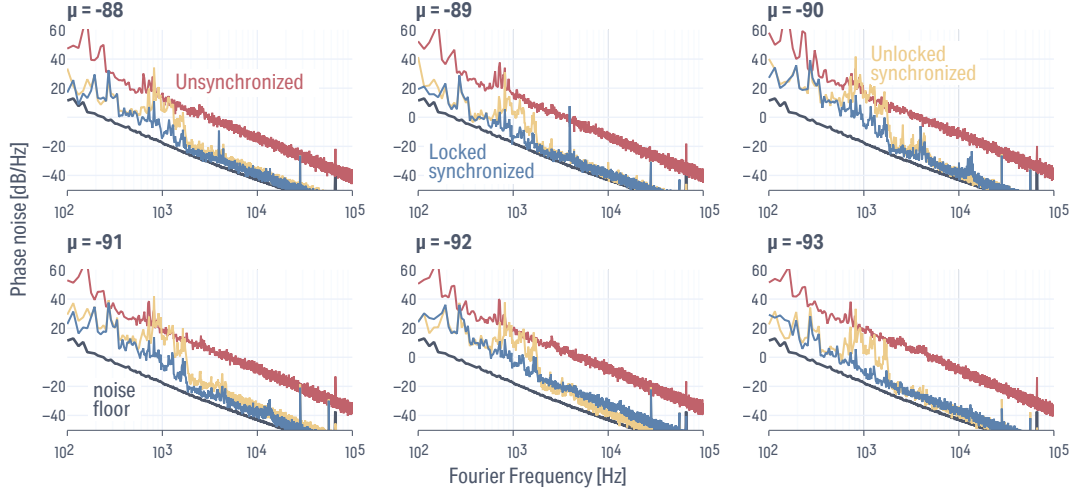


Fig. S4 – Frequency noise of several single microcomb OFC teeth measured using the MZI apparatus from Section S-4, while having the reference at $\mu_s = -94$. In red, we display the unsynchronized case (*i.e.* no reference present in the system), in yellow the synchronized system with all lasers being free running, and in blue the synchronized system with locked lasers. The power is referenced to the carrier, *i.e.*, dBc/Hz.

S-6. Soliton self-balancing under Kerr-induced synchronization

The dynamics of self-balancing of the soliton in the KIS regime can be easily understood through a simplified explanation of the underlying physics. Firstly, it is important to remember that the observed DWs (dispersive waves) in the microcomb spectra are oscillatory tails in the cavity coordinate, with the red DW trailing behind the blue DW [Fig. S5a]. As mentioned earlier, the KIS regime is favored, though not limited to, modes where the integrated dispersion is minimized and is therefore close to the DW. Once synchronized, the reference laser captures a comb tooth, causing the dropped reference pump laser to become the oscillatory tail in the intracavity profile, significantly increasing its amplitude [Fig. S5a]. As a result, the center of mass of the DKS is shifted. However, in this regime, the main pump and reference pump pin two of the microcomb teeth, fixing the repetition rate of the DKS. As a consequence of the conservation of the first moments, the fixed repetition rate results in a fixed center of mass in time. The soliton must adapt and self-balance to meet this condition. Since the shape of the soliton envelope is directly related to the dispersion of the resonator, the only degree of freedom the soliton has to self-balance is by increasing its

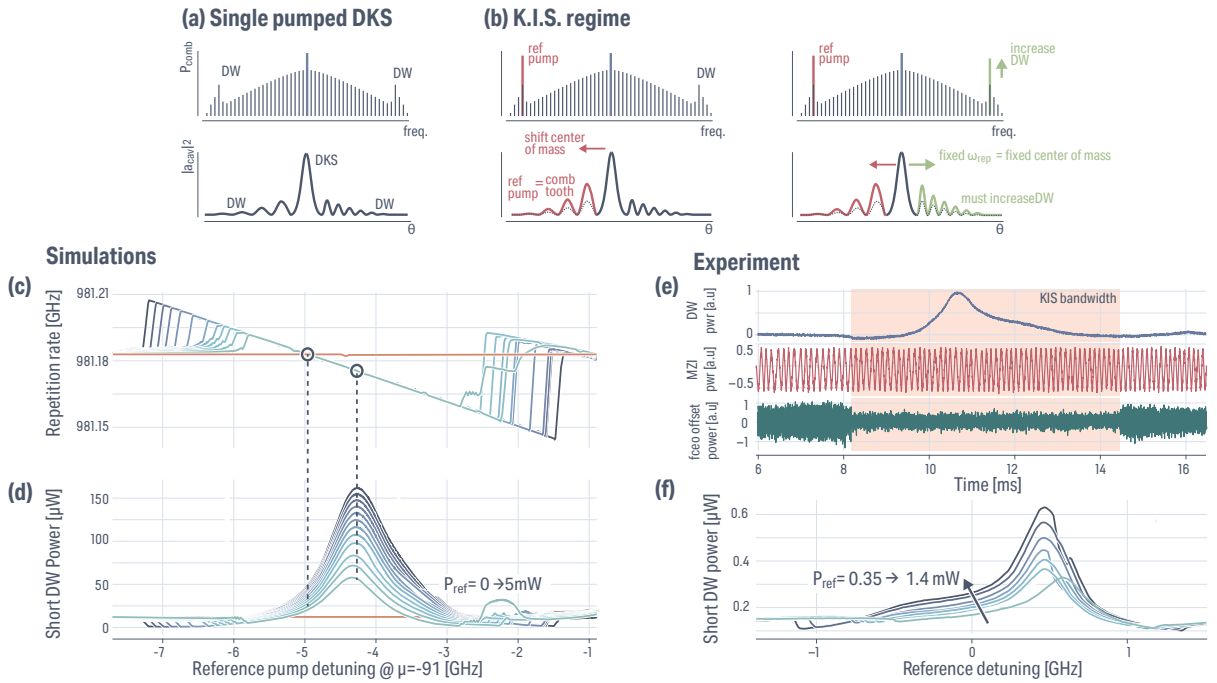


Fig. S5 – **a** Reminder of the relationship between the spectrum and intracavity profile of the DKS. **b** Toy model to understand the self-balancing effect in KIS. The reference pump becoming a DW increases the oscillatory tail amplitude of the DKS. However, the repetition rate being fixed, the center of mass must be constant in time, and hence the soliton must self-balance by increasing radiation in the other DW. **c** Simulation of the repetition rate variation with reference pump power variation (lighter to darker = lower to higher reference pump power). **d** Simulation of the opposite DW comb tooth power from the reference with reference pump frequency tuning and power. The bump in the profile corresponds to the optimal phase matching condition from the repetition rate tuning, and the increase of the DW power with the reference power is a signature of self-balancing. **e** Experimental measurement of the short wavelength DW power using an 800 nm short pass filter (blue) and calibrating the frequency sweep with a MZI (red) and AC-coupled photodiode detection of the CEO mismatch between the reference pump and the nearest comb tooth (green). **f** Experimental demonstration of self-balancing of the short wavelength DW with C-band reference pump.

radiation into the other oscillatory tail, thereby enhancing the power of the opposite DW from which synchronization occurs.

Mathematically, this effect is apparent from either Eq. (S.10), where the conservation of the repetition rate in time can only be balanced by K_{NL} for any change of P_{ref} , or in Eq. (S.15), where the left-hand side must remain null in the synchronized case even for variations in P_{ref} , where the opposite sign between \mathcal{T} and K_{NL} emphasizes the increase of the short DW to remain synchronized.

We verify this theoretically by performing LLE simulations and probing the DW azimuthal component power with the change of the reference pump power and frequency detuning. First, in the KIS regime, the repetition rate is tuned by the reference pump frequency tuning [Fig. S5c]. This allows us to change the phase-matching condition of the azimuthal component with the cavity resonance (see the next section for more detail). Hence, an optimum repetition rate exists for which the DW is maximized for any reference pump power, as seen in Fig. S5d. However, for any given phase-matching condition of the DW component, its power is dependent on the reference pump power, emphasizing the self-balancing effect and the robustness of the soliton.

We measure this effect experimentally using the fast (50 Hz) piezo element of the CTL laser, allowing for fine tuning of the reference pump laser. Using an 800 nm short pass filter, we record the short DW power while synchronizing with the reference pump in the C-band. We also record the transmission of the reference pump through a 40 MHz Mach-Zehnder interferometer for frequency calibration of the scan and the measured beat between the reference pump and the closest comb tooth [Fig. S5e]. In the KIS regime, this beating is null, so coupling the photodiode in AC mode allows us to retrieve the KIS bandwidth in the absence of a beat signal.

Using a tunable attenuator, we vary the on-chip reference pump power from 350 μ W to 1.4 mW and observe the same behavior as the theory predicts, namely optimization of the phase matching at a given reference pump frequency while observing an increase of the short wavelength DW power with the reference pump laser.

S-7. Dispersive wave tuning from repetition rate tuning under the KIS regime

As discussed in the previous section, the DW phase matching condition can be tuned by the reference pump frequency tuning. The change of repetition rate allows for the azimuthal component at μ_{DW} to be more or less phase matched with the cavity resonance such that with optimum when $\beta_{\text{DKS}}(\omega) = \beta_{\text{res}}(\omega)$, which from the discrete set μ of linear resonance $\beta_{\text{res}}(\omega) = 2\pi R(\mu + \mu_0)$ where μ_0 is the main pumped mode and R the resonator radius. Hence, the phase matching condition can be simply transformed into a frequency condition one such that $\omega(\mu_{\text{DW}}) - \omega_{\text{rep}}\mu_{\text{DW}} = 0$, where μ_{DW} is the dispersive wave fulfilling this condition. When $\omega_{\text{rep}} \equiv D_1$ with D_1 the linear free spectral range at the main pump, this phase matching condition is the integrated dispersion $D_{\text{int}}(\mu)$, where its zero crossing exhibit phase matching hence DW enhancement.

In the KIS regime, the change of the repetition rate allows for tuning of the phase matching condition. Interestingly, if the change of repetition rate is large enough, one could tune into phase matching different azimuthal mode μ around the linear DW mode μ_{DW} . We explore this possibility through LLE simulation using a 10 mW reference pump power. As expected, the repetition rate is changing linearly with the reference pump detuning [Fig. S6a]. Probing four different modes, the original DW mode μ_{DW} and up to three modes lower ($\Delta\mu_{\text{DW}} = -3$), we see that the enhancement alternates based on the repetition rate of the DKS. In the microcomb spectra, this translates to the possibility to pick the mode that will experience DW enhancement [Fig. S6c-d], which can find application in tuning of microcomb tooth power for interfacing, for instance, to atomic systems.

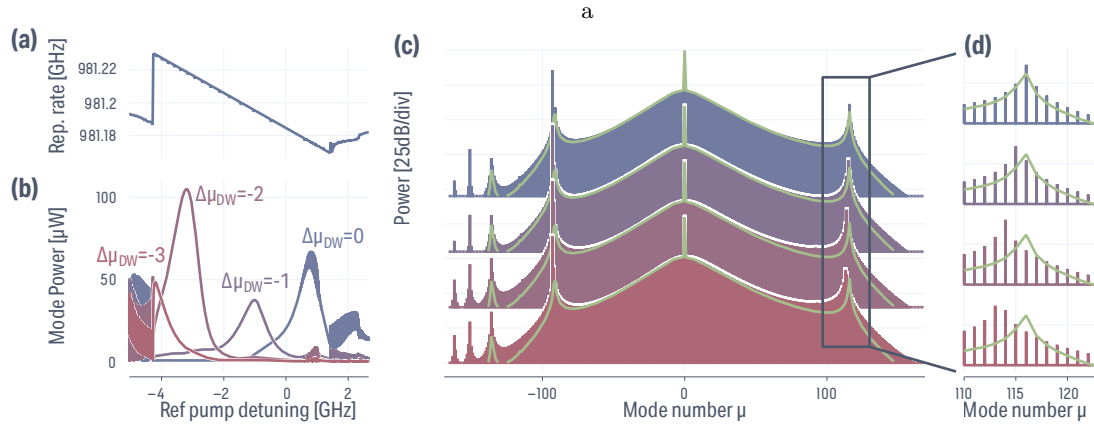


Fig. S6 – **a** Simulated repetition rate tuning with a reference pump power of 10 mW at $\mu_{\text{DW}} = -90$. **b** Power of different comb teeth, with $\Delta\mu_{\text{DW}} = 0$ being the nominal DW mode without reference pump at $\mu = 116$ and $\Delta\mu_{\text{DW}} = X$ is X comb teeth away. **c** Comb spectra for reference pump detuning corresponding to the maximum of power of $\Delta\mu_{\text{DW}} = 0$ (blue) up to $\Delta\mu_{\text{DW}} = 3$ (red). The comb envelope under single pumping (no KIS) is shown in green. **d** Zoom-in at the short wavelength DW (opposite from the reference pump), highlighting the tuning of the DW with the reference pump frequency.

-
- [1] Moille, G. et al. Two-Dimensional Nonlinear Mixing Between a Dissipative Kerr Soliton and Continuous Waves for a Higher-Dimension Frequency Comb. [arXiv](#) (2023). 2303.10026.
 [2] Couillet, P., Gilli, J. M., Monticelli, M. & Vandenberghe, N. A damped pendulum forced with a constant torque. [American Journal of Physics](#) **73**, 1122–1128 (2005).